Diagnostic and Interventional Imaging 104 (2023) 567–583

Review/*Musculoskeletal imaging*

Radiomics and artificial intelligence for soft-tissue sarcomas: Current status and perspectives

Amandine Crombé[a,b,c,*], Paolo Spinnato[d], Antoine Italiano[e], Hervé J. Brisse[f], Antoine Feydy[g,h], David Fadli[a], Michèle Kind[b]

[a] *Department of Radiology, Pellegrin University Hospital, 33000 Bordeaux, France*
[b] *Department of Oncologic Imaging, Bergonié Institute, 33076 Bordeaux, France*
[c] *'Sarcotarget' team, BRIC INSERM U1312 and Bordeaux University, 33000 Bordeaux France*
[d] *Diagnostic and Interventional Radiology, IRCCS Istituto Ortopedico Rizzoli, Bologna 40136, Italy*
[e] *Sarcoma unit, Bergonié Institute, 33076 Bordeaux, France*
[f] *Imaging Department, Institut Curie, 75248 Paris, France*
[g] *Department of Radiology, Hopital Cochin-AP-HP, 75014 Paris, France*
[h] *Université Paris Cité, Faculté de Médecine, 75006 Paris, France*

ARTICLE INFO

Keywords:
Artificial intelligence
Magnetic resonance imaging
Radiomics
Soft-tissue sarcomas
Soft-tissue tumors

ABSTRACT

This article proposes a summary of the current status of the research regarding the use of radiomics and artificial intelligence to improve the radiological assessment of patients with soft tissue sarcomas (STS), a heterogeneous group of rare and ubiquitous mesenchymal malignancies. After a first part explaining the principle of radiomics approaches, from raw image post-processing to extraction of radiomics features mined with unsupervised and supervised machine-learning algorithms, and the current research involving deep learning algorithms in STS, especially convolutional neural networks, this review details their main research developments since the formalisation of 'radiomics' in oncologic imaging in 2010. This review focuses on CT and MRI and does not involve ultrasonography. Radiomics and deep radiomics have been successfully applied to develop predictive models to discriminate between benign soft-tissue tumors and STS, to predict the histologic grade (*i.e.*, the most important prognostic marker of STS), the response to neoadjuvant chemotherapy and/or radiotherapy, and the patients' survivals and probability for presenting distant metastases. The main findings, limitations and expectations are discussed for each of these outcomes. Overall, after a first decade of publications emphasizing the potential of radiomics through retrospective proof-of-concept studies, almost all positive but with heterogeneous and often non-replicable methods, radiomics is now at a turning point in order to provide robust demonstrations of its clinical impact through open-science, independent databases, and application of good and standardized practices in radiomics such as those provided by the Image Biomarker Standardization Initiative, without forgetting innovative research paths involving other '-omics' data to better understand the relationships between imaging of STS, gene-expression profiles and tumor microenvironment.

1. Introduction

Soft-tissue sarcomas (STS) are malignant mesenchymal tumors characterized by their ubiquity and by the diversity of their clinical, histological, molecular and radiological presentations [1]. This subsequent heterogeneity on imaging from one patient to another patient has naturally prompted researchers and physicians to question whether these distinct radiological phenotypes (or 'radiophenotypes') had biological correlates and were associated with relevant oncologic outcomes.

Classical radiological analyses of STS (also named 'semantic' analyses), defined as the assessment of explainable traits by experienced radiologists depicting the tumor aspect (for instance, the

Abbreviations: ADC, Apparent diffusion coefficient; ALT, Atypical lipomatous tumor; CE, Contrast-enhanced; CNN, Convolutional neural network; ΔRF, Delta radiomics features; ESMO, European Society of Medical Oncology; FS, Fat-suppressed; FNCLCC, French Federation of Cancer Centers; IBSI, Imaging Biomarker Standardization Initiative; LFS, Local relapse-free survival; MDTB, Multidisciplinary tumor board; MFS, Metastatic relapse-free survival; NACT, Neoadjuvant chemotherapy; NART, Neoadjuvant radiotherapy; OS, Overall survival; PET/CT, 18-fluorodeoxyglucose positron emission tomography/computed tomography; RECIST, Response evaluation criteria in solid tumor; RF, Radiomics feature; RQS, Radiomics quality score; SI, Signal intensity; STS, Soft tissue sarcoma; STT, Soft tissue tumor; WI, Weighted imaging

* Corresponding author.
E-mail address: amandine.crombe@chu-bordeaux.fr (A. Crombé).

https://doi.org/10.1016/j.diii.2023.09.005
2211-5684/

visualization of peritumoral edema on MRI), has considerably improved over the last decades. For instance, previous studies have identified semantic features associated with malignancy (notably when facing a myxoid soft-tissue tumor or an adipocytic tumor), higher histologic grade and lower survivals [2–7]. However, semantic analyses are also limited by their (mainly) qualitative nature and their moderate intra- and inter-observer reproducibility. For instance, peritumoral enhancement on contrast-enhanced (CE) fat-suppressed (FS) T1-weighted imaging (WI) has been stressed as strongly associated with higher grade, lower metastatic-relapse free survival (MFS) and overall survival (OS) and but its kappa index was 0.62, which questions its usefulness in clinical practice and its acceptability during decision making by multidisciplinary tumor board (MDTB) [2]. Furthermore, STS may appear heterogeneous on MRI due to different intra-tumoral patterns that can be difficult to capture with human eyes and to explain with human words. Consequently, so far, the main radiological features considered by MTDBs and prognostic nomograms (such as the Sarculator) remain the tumor size, depth, location, and relationships to nerves, major vessels, and bones [8,9].

Radiomics is a growing field of research in imaging that could help solving these issues by providing tools to quantify the STS radiophenotype massively, objectively and without *a priori,* on any imaging modality. The term appeared in 2010 [10], and has spread to the sarcoma research in 2015 [11], mostly on 18F-fluorodeoxyglucose positron emission tomography/computed tomography (PET/CT), MRI and CT. The concepts and methods have been extensively described in previous reviews [12–14]. Overall, following the post-processing of medical images (in order to ensure their comparability and to reduce biases due to technical characteristics unrelated to the disease), several numeric features (*i.e.,* the radiomics features [RFs]) quantifying the shape and the texture (*i.e.,* the spatial inter-relationships of gray

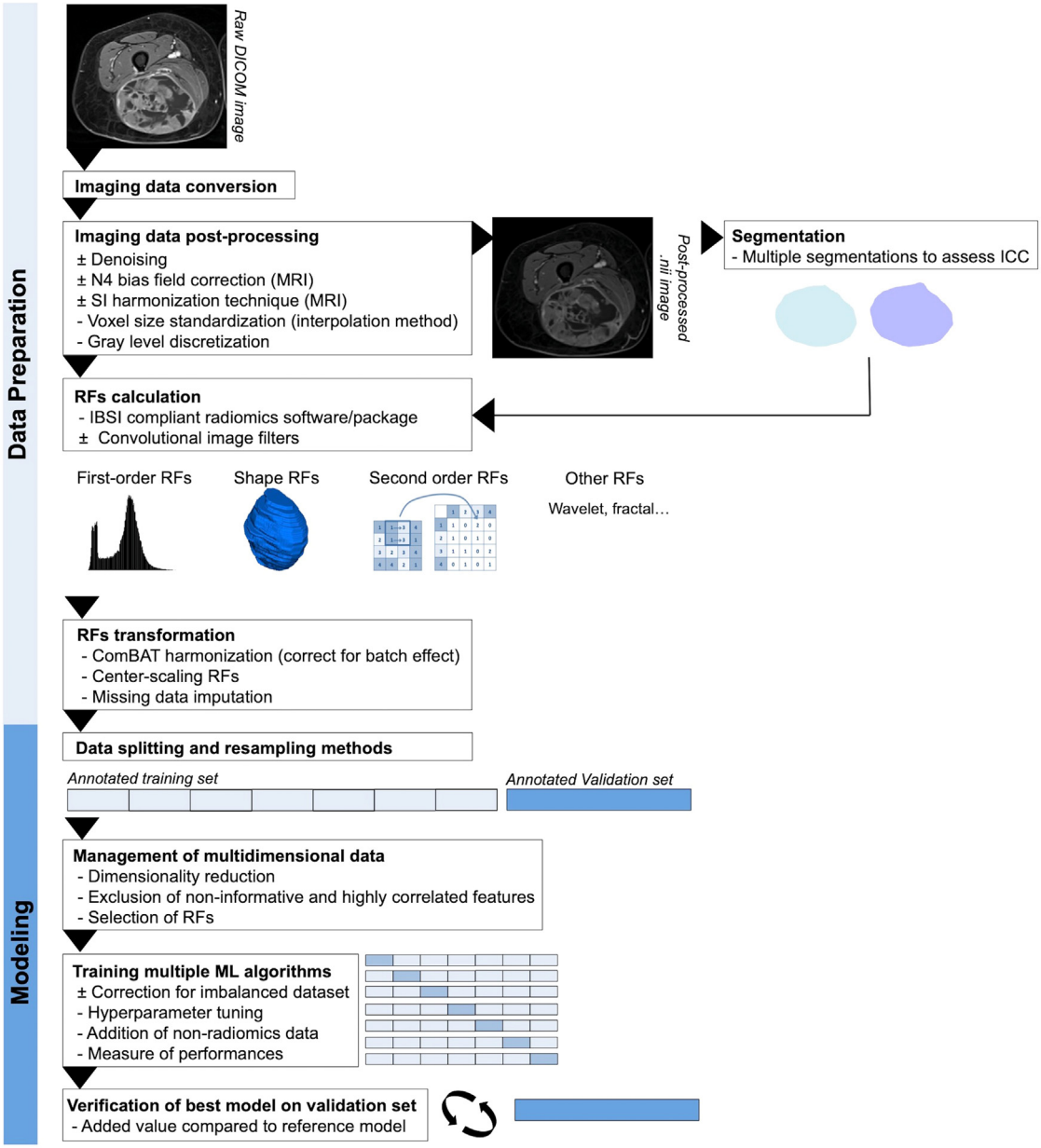

Fig. 1. Principle of the development of a radiomics model.
IBSI indicates Image Biomarker Standardization Initiative; ICC indicates intraclass correlation coefficient; ML indicates machine learning; RF indicates radiomics feature; SI indicates signal intensity.

levels) are extracted from tumor segmentation using mathematical operators encoded inside radiomics softwares and packages. Those radiomics features can then be used to achieve unsupervised classification of STS thanks to clustering algorithms, or mined as potential predictors for a precise outcome within supervised analysis. Because of the marked collinearity and multidimensionality in radiomics dataset, specific machine-learning methods involving handcraft and engineered steps are required to avoid false discoveries and over-optimistic results. More recently, the implementation of deep learning algorithms on sarcoma imaging could even increase the potentialities of imaging to improve the management of STS patients through.

Thus, after a brief reminder of the quality criteria for establishing an efficient and reproducible radiomics models, this review aims at explaining the rationale for applying radiomics in STS patients and the main findings regarding diagnosis, prognostication, response assessment and follow-up. Although radiomics can apply on any imaging modality and ultrasonography remains the first-line imaging in most patients, this review strictly focuses on CT and MRI. Finally, we will list the expected developments in the field of radiomics and artificial intelligence, namely, better explainability, better quantification and easier and practical applications for STS patients.

2. Understanding radiomics approaches

Radiomics belong to '-*omics*' data and approach, and share the same paradigm, pros and cons. The mandatory technical steps to apply and report in radiomics studies have been formalized by the Imaging Biomarker Standardization Initiative (IBSI), an independent international collaboration committed to the high quality and reproducibility of imaging biomarkers and high-throughput image analysis [15,16]. Additionally, the radiomics quality score (RQS) proposes to quantify the quality and reliability of a radiomics models based on 16 items, which represent a framework for researchers in radiomics [12]. The important points from the IBSI recommendations and RQS are precisely detailed at https://ibsi.readthedocs.io/en/latest/04_Radiomics_reporting_guidelines_and_nomenclature.html. Fig. 1 illustrates those main steps of the building of a radiomics model.

First, radiomics approaches require methods to ensure the comparability of imaging acquired at different time points on different systems from different centers before extracting RFs. Hence, quality controls and imaging post-processing steps are needed to remove potential biases. Various steps with different options or arguments can be tested (denoising, N4 bias field correction, signal intensity homogenization, voxel size resampling and interpolation, type of discretization, ComBat harmonization) and must be reported in methods to make the radiomics models replicable [17].

Obviously, standardizing protocols for soft-tissue tumors (STT) is highly recommended to reduce the exclusion of patients, the measurement biases and too complex post-processing at risk of removing relevant information, especially for MRI, which is the best and recommended imaging modality for local staging of STS and the most frequently used in radiomics studies involving STS (69.2% of radiomics publications about STS) [18]. Table 1 proposes such standardized protocol as performed in our centers a compromise between clinical usefulness and proposals from the European Organization for the Research and Treatment of Cancer and the European Societal of Skeletal Radiology – although no international consensus has been validated [19].

Second, the extraction of RFs requires good quality segmentation of the objects of interest (herein, STS volume, but also possibly their surrounding tissues or metastases) [20]. Today, the segmentation of STS remains performed manually (or semi-automatically), which is tedious and time-consuming and can influence the values of radiomics features. Consequently, it is good practice to evaluate the inter-segmentation reproducibility of radiomics features and to remove those too sensitive to segmentation perturbations expected in clinical practice. Generally, a threshold between 0.80 and 0.90 for inter-segmentation intra-class correlation coefficients is applied to filter the reproducible features.

This extraction also requires radiomics software and package using standardized definitions and formula, and compliant with the IBSI guidelines [15].

The third step corresponds to the utilization of the RFs in supervised or unsupervised analyses. In supervised analyses, the aim is to predict a well-defined outcome (in our setting: benign STTs or STS, histologic or molecular features, response to neoadjuvant chemotherapy or radiotherapy [NACT, NART] and survivals). Thus, it is crucial to start from multi-centers, large and well-labeled cohorts of patients to train the supervised machine-learning algorithms and their hyperparameters (i.e., a parameter that is fixed before the training and that controls the learning process, thanks to tuning grids), using resampling schemes such as repeated cross-validation, and then to verify the performances of the best models on an independent test set. The aim of the model must be well defined to determine the performance metrics to select the best model. Other essential statistical steps include: (*i*), methods to correct for imbalanced datasets (such as oversampling the minority class or generating synthetic observations); (*ii*), methods to reduce the dimensionality (such as principal component analysis) and to select variables (such as

Table 1
Proposal for MRI protocol for soft-tissue sarcoma.

Sequence		Remark
Sytematic	Coronal or sagittal STIR T2 TSE	Should include the whole anatomical segment to look for multifocal lesions and evaluate peritumoral edema
	Axial T1 TSE[1]	Can be replaced by a single axial T1-weighted TSE Dixon with fat, in and water image
	Axial FS T1 TSE[1]	
	Axial T2 TSE[1]	–
	Axial contrast-enhanced FS T1 TSE[1]	Should be subtracted with pre-contrast image; FS can be replaced by Dixon
	Coronal or sagittal contrast-enhanced FS T1 TSE	Should include the whole anatomical segment to look for multifocal lesions and evaluate peritumoral enhancement
Optional	Axial DWI	b = 0, 400 and 800–1000s.mm^{-2}; calculation of ADC map with monoexponential model
	T1 mapping	At least 2 variable flip angle = 2° and 15°[2]
	T2 mapping	Multiple TE sequence
	DCE-MRI FS FSPGR T1	Calculation of semi-parametric and parametric maps (after applying Tofts-Kety model)
	3D isotropic T1 GRE Dixon	for multiplanar reconstruction and surgery planning

ADC indicates apparent diffusion coefficient; DCE indicates dynamic contrast-enhanced; DWI indicates diffusion-weighted imaging; FS indicates fat-suppressed; FSPGR indicates fat-spoiled gradient; GRE indicates gradient-recalled echo; STIR indicates short tau inversion recovery; TE indicates echo time; TSE indicate turbo spin-echo.
[1] All axial sequences should use the same resolution and be coregistered, for better voxel-wise analysis.
[2] According to the quantitative imaging biomarker alliance, T1-mapping enables better estimation of the parametric DCE-MRI parameters.

univariable filter or recursive filter analysis or penalized methods); *(iii)*, verification of the good calibration of the model (*i.e.*, that the predicted class probabilities are consistent with the rates of observed events); *(iv)*, retrospective analysis of the observations with recurrent prediction errors in order to find clues to improve the model; and *(v)*, verification of the added value of the model compared to pre-existing clinical, histologic or and semantic radiological models.

In unsupervised analyses, the RFs are included into clustering algorithms (for instance k-means or hierarchical clustering) to generate classifications of the tumors without *a priori* knowledge, and to discover hidden patterns within a dataset. Afterwards, associations with histological and molecular features of STS are generally performed.

Lastly, clinical researchers are beginning to implement deep learning algorithms on imaging of STS for the following tasks (Fig. 2): *(i)*, Prediction: instead of returning 2D or 3D segmentation or the initial image, the last fully-connected and output layers of the model can provide a binary or multiclass classification or a survival

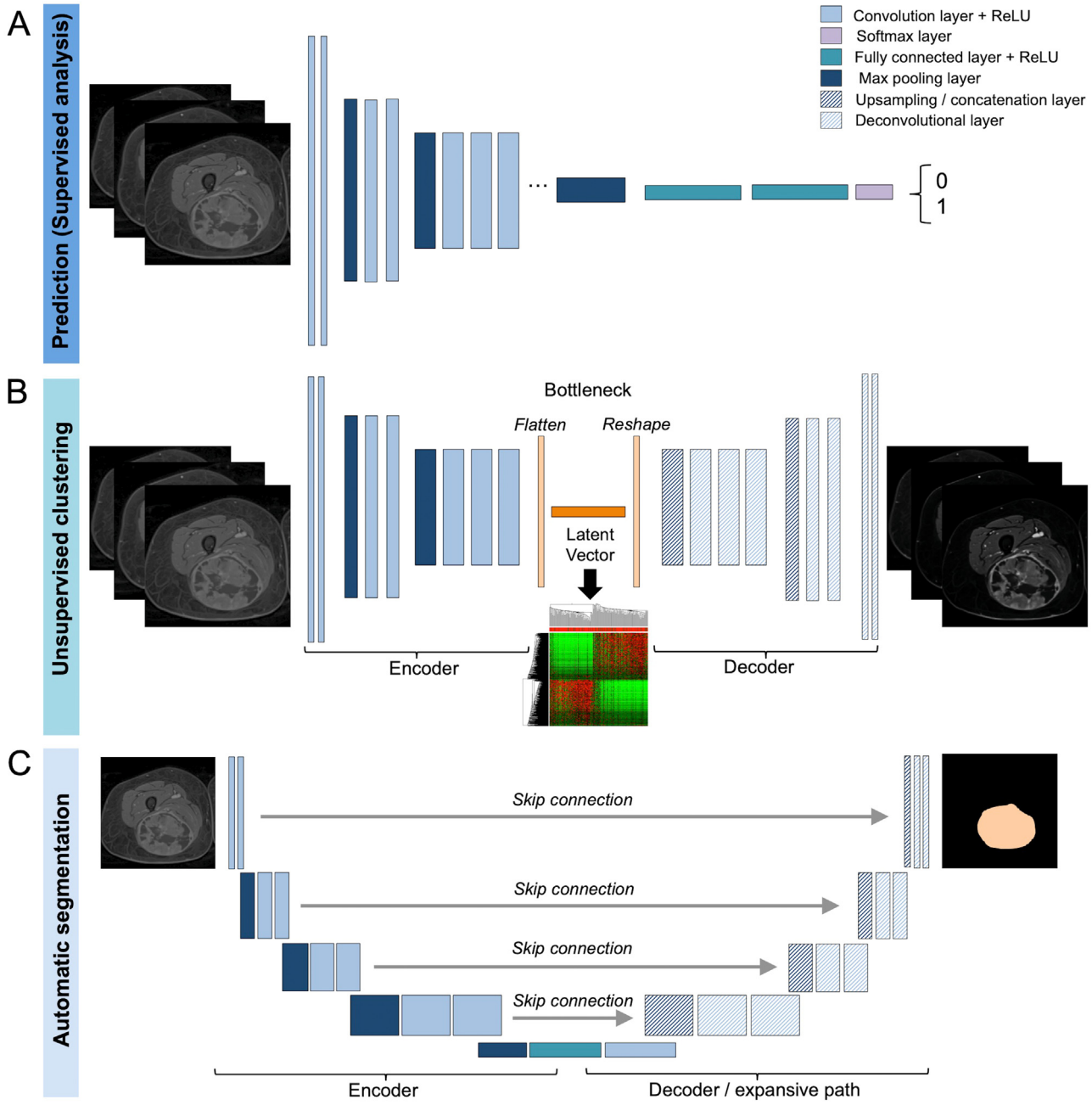

Fig. 2. Principle of deep learning in research involving imaging of soft-tissue sarcoma. (A) For supervised analysis, convolutional neural network (CNN) are made of a succession of (i) convolutional layers with small convolution filters and activation function such as rectified linear unit (ReLU) and (ii) max pooling layers that downsample a feature map (i.e., output of the convolutional layer) by calculating the maximal value of a patch from it. It ends with (iii) fully connected layers (to combine information from each input of the prior layer) and lastly (iv) softmax layer to provide probability for each category of the desired classification. (B) Deep learning can also help for unsupervised classification thanks to autoencoder CNN, of which, basically, the aim is to reproduce as well as possible the input image as output. To do so, it adds a decoder part to the 1st encoder part (similar to the 1st part of classical CNN) made of upsampling layer and deconvolutional layer in order to replicate the input based on the highly informative latent vector in the bottleneck of the network. Once the autoencoder is operational, the features of the latent vector can be extracted and used to generate unsupervised classification. (C) Semantic automatic segmentation is achieved with architecture similar to U-NET CNN, which is partly similar to autoencoder CNN, except that skip connections provide information to the decoder/reconstruction part about the location of the features captured with the convolutional layers from the encoder part.

prediction; *(ii),* Unsupervised analyses: thanks to autoencoder CNNs (whose aim is to reproduce as best as possible the input image), it is possible to extract thousands of highly-informative numeric features from the latent layer at the bottleneck of the network (also named deep-RFs) that can be secondarily included in clustering algorithms; and *(iii),* Segmentations: thanks to 3D U-NET convolutional neural network (CNN) or Efficient neural network and their derivatives, it is technically possible to segment tumors in 3D, and secondarily, to automatically achieve radiomics pipelines on those segmentations;

Those algorithms are generally pre-trained on large image datasets (such as the ImageNet image collection, https://www.image-net.org/), and adapted to the researchers' objectives thanks to transfer learning and fine tuning and re-training of the last layers [21]. Popular re-usable algorithms include VGG16, VGG19, ResNet-50, Efficient neural network, or InceptionV3. In this review, articles with univariable analysis only were not considered.

3. Discriminating benign and malignant tumors

3.1. Generalist models

Benign STTs strongly outnumber STS, although the benign/malignant ratio markedly decreases from 100/1 to 7/1 for STS larger than 5 cm [22]. Semantic radiological analyses of STS and benign STTs show important overlap, which has encouraged radiologists to investigate alternative methods to deepen their characterization including radiomics. One of the oldest radiomics studies, by Juntu et al., actually trained machine learning algorithms (support vector machine, artificial neural network, and decision trees) on textural features from 2D-squared region-of-interest from T1-WI of a single-center retrospective cohort of 135 patients with STTs, this before the term 'radiomics' was proposed [23]. Then, they compared the best model (which relied on support vector machine) predictions with the radiologists' predictions and concluded on the highest performances of the support vector machine model (accuracy = 93% and area under the ROC curve [AUC] = 0.92, *vs.* accuracy = 90% and AUC = 85% for radiologists). Although this study lacked of external validation and reproducibility assessment, these results have been confirmed by three other radiomics studies relying on T1-WI, contrast-enhanced (CE) T1-WI, T2-WI, and proton density WI (best model using ADABOOST algorithm with AUC = 0.77) [24], apparent diffusion coefficient (ADC) map (best model using random forests, AUC = 0.77–0.81) [25], and T2-WI and CE-T1-WI (best model using least absolute shrinkage and selection operator logistic regression, AUC = 0.95) [26] for a total of 553 patients (Table 2).

However, systematic methodological limitations must be noted, namely: retrospectivity, lack of available code, and, subsequently, no comparison with the models proposed by other groups (and against radiologists' conclusion in 2/4 [50%] studies), or no mention of MRI pre-processing before radiomics in 3/4 (75%) studies.

Critics regarding radiomics model for predicting malignancy for any STT, without considering obvious discriminative tumor characteristics such as presence of myxoid signal or adipocytic signal (which will restrict the histologic possibilities), have prompted researchers to develop models to predict malignancy for these subgroups.

3.2. Atypical lipomatous tumors (ALT) versus lipoma

Lipoma is the most frequent soft tissue tumor [27]. Differentiating ALT (or well-differentiated liposarcoma, a locally aggressive STS that may evolve towards dedifferentiated liposarcoma) from lipoma is highly challenging for radiologists and pathologists on hematoxylin and eosin stained slices, and require a tissue sample to identify the amplification of the MDM2 gene thanks to fluorescence in situ hybridization [1]. Yet, biopsying all homogeneous lipomatous tumors to perform MDM2 fluorescence in situ hybridization would be unfeasible and highly expensive. Simple algorithms to stratify patients' management relying on tumor depth, size and feasibility of re-resection did not specifically address this diagnostic challenge [19,27]. Therefore, radiomics models have been developed by several research groups and recently summarized by Haidey et al., who concluded on a sensitivity of 68–100% and a specificity of 33–100% for these models [28]. Table 3 lists the main 12 studies for a total of 1323 patients. One was based on CT and conventional MRI, and 11 on conventional MRI alone. All used conventional texture and shape RFs and two also investigated deep RFs from pre-trained ResNet50 CNN [29,30]. The conclusions of these two studies using deep RFs were different: one suggesting the superiority of deep RFs over handcrafted RFs and clinical model [29], whereas the other study found the highest performances with batch-corrected handcrafted RFs [30]. One study also included semantic radiological features (location, depth, and septation) in a composite model to reach its highest performance (AUC = 0.80) [31]. It can be noted that two of the latest studies (achieved on the largest populations) found the highest accuracy on the independent test set with the radiological analysis from a senior radiologist against radiomics model, namely: accuracy = 90% versus 76%, respectively, according to Foreman et al. [32], and accuracy = 64% *vs.* 53%, respectively, according to Gitto et al. [33]. All models demonstrated high diagnostic performances whatever the finally selected machine learning algorithms and input data, with AUC ranging from 0.80 to 0.97 in an independent testing cohort [34], with the same limitations as for 'benign vs. malignant' models, including a lack of models' explainability and understanding of its failures and outliers. Thus, although encouraging, those studies remain retrospective proof-of-concepts without practical applications.

4. Predicting grade and other initial histopathologic features

The histologic grade by the French Federation of Cancer Centers (FNCLCC) is one of the strongest predictors of STS patients' OS and MFS [35]. In the European Society of Medical Oncology (ESMO), the grade is a stratifying variable to decide the optimal therapeutic strategy for locally-advanced STS [8]. This is a 3-tier system including assessment of the amount of necrosis, differentiation and mitosis on the entire tumor tissue [36]. With the development of imaging-guided biopsy, the grade is now assessed on small tissue samples, which can cause underestimation in 12.3–55% of patients [2]. Since MRI provides an overview of the entire volume and since conventional MRI features have been associated with grade (in particular the signal intensity [SI] heterogeneity on T2-WI, the amount of necrosis and the presence of peritumoral enhancement on CE-T1-WI in multivariable analysis, named '*radiology signature*' when at least 2 out of these 3 features were present) [2,3], researchers have naturally investigated radiomics approaches to predict the real grade of STS (Fig. 3). Table 4 summarizes the main studies for this classification task, for a total of 1305 patients, although it must be underlined that (*i*), some defined high grade as grade III tumor only whereas others defined high grade as grade II and III, and (*ii*), some used the grade estimated on biopsy or after neoadjuvant treatment as the reference and not the grade on the full untreated surgical sample. All those studies were based on conventional MRI (with T2-WI ± fat suppression being constantly evaluated) except for one study on the apparent diffusion coefficient (ADC) map of 19 patients [37]. Two studies also assessed deep RFs (extracted from a single representative slice, or 4 slices pasted side-by-side on square 2D-image) from various types of CNNs to feed machine learning classifiers [38,39]. The resulting AUC were 0.77–0.92 in training cohorts and 0.76–0.87 in validation cohorts, and, were systematically higher than the AUCs of the analyses performed by radiologists (although none compared the '*radiology signature*', described above) [2,3].

Table 2
Main radiomics studies regarding the discrimination between benign and malignant soft-tissue tumors (STTs).

Author [ref. #]	Imaging modality	No. of patients in training cohort	No. of patient in test cohort	Best model	Performances in training cohort	Performances in validation cohort	Main limitations
Juntu et al., 2010 [23]	MRI (T1)	135 pts from one center (49 malignant tumor). Radiomics analysis was achieved on multiple square ROIs of 50 × 50 pixels per tumor (253 benign ROIs and 428 malignant ROIs)	–	Non linear Vapnik's SVM	AUC = 0.91, accuracy = 93%, outperformed radiologists (AUC = 0.85, accuracy = 90%)	–	Retrospective; Single center; No resampling scheme; No MRI harmonization; 2D square ROIs at risk of sampling bias; No IBSI-compliant software; No reproducibility analysis; No available code
Fields et al., 2021 [24]	MRI (T1, CE-T1, T2, proton density ± fat suppression)	128 pts from one center (92 malignant tumors)	–	ADABOOST on all MR sequences	AUC = 0.77	–	Retrospective; Single center; No independent test set; No MRI harmonization; No IBSI-compliant software; No reproducibility analysis; No comparison with reference model/radiologists; No available code
Lee et al., 2021 [25]	MRI (ADC)	105 pts from one center (47 malignant tumors)	46 pts from the same center (24 malignant tumors)	Random forests classifier based on radiomics features + ADC minimum + ADC mean	AUC = 0.841 & 0.860 (analyses performed twice, depending on the segmentation of two radiologists)	AUC = 0.775 & 0.807 (analyses performed twice, depending on the segmentation of two radiologists) not significantly better than simple ADC minimum value (AUC = 0.711 and 0.753)	Retrospective; No comparison with radiomics model built with conventional MR sequence; No available code
Yue et al., 2022 [26]	MRI (T2 with fat suprression, CE T1)	91 pts from one center (36 malignant tumors)	48 pts from the same center (18 malignant tumors)	Nomogram combining clinical and radiological features (size, peritumoral edema, margin delineation), and radiomics score developed on CE-T1 and fat suppressed T2 after filtering RFs thanks to univariable Mann-Whitney test, then selecting them with LASSO, then applying a stepwise logistic regression based on AIC	AUC = 0.962 in cross validation for the nomogram, outperformed the radiomics score alone and clinical-radiological model alone (both AUC = 0.923)	AUC = 0.935 for the nomogram, outperformed the radiomics score alone (AUC = 0.892) and clinical radiological model alone (AUC = 0.827)	Retrospective; Small dataset; No independent test set; No resampling scheme; No available code

ADC indicates apparent diffusion coefficient; AIC indicates Akaike information criterion; AUC indicates area under the ROC curve; CE indicates contrast enhanced; IBSI indicates imaging biomarker standardization initiative; LASSO indicates least absolute shrinkage and selection operator; No. indicates number; pts indicates patients; RF indicates radiomics feature; ROI indicates region of interest; SVM indicates support vector machine.

Table 3
Main radiomics studies regarding the discrimination between lipoma and liposarcoma / atypical lipomatous tumors (ALTs).

Author [ref. #]	Imaging modality	No. of patients in training cohort	No. of patient in test cohort	Best model	Performances in training cohort	Performances in validation cohort	Main limitations
Thornhill et al., 2014 [66]	MRI (T1)	44 pts from 1 center (20 liposarcomas)	–	Linear discriminant anlysis trained on 3 texture and 3 shape features selected according to Fisher coefficient	AUC = 0.98, outperformed the two radiologists (AUC = 0.88 & 0.89)	–	Retrospective; Single center; Small dataset; Inclusion of myxoid liposarcoma, dedifferentiated liposarcoma and pleomorphic liposarcoma; No independent test set; No MRI harmonization; No IBSI-compliant software; No (radiomics) reproducibility analysis; No available code
Vos et al., 2019 [67]	MRI (T1, T2)	116 pts from 1 center (58 ALTs) + 22 dedifferentiated liposarcoma	–	Ensemble method based on top-50 best performing algorithms among logistic regression, SVM, naive Bayes, random forests, linear and quadratic discriminant analysis trained on RFs (after selection and PCA) from T1 and T2	AUC = 0.89 (and 0.81 after volume matching), outperformed the radiologists (AUC = 0.61−0.74).	–	Retrospective; Single center; No independent test set; No reproducibility analysis
Pressney et al., 2020 [31]	MRI (proton density, T1)	60 pts from 1 center (30 ALTs)	–	Score combining the four following dichotomized variables: location, depth, septation/non fat content, and one radiomics feature from proton density	AUC = 0.80	–	Retrospective; Single center; Small dataset; No independent test set; No resampling scheme; No MRI harmonization; No IBSI-compliant software; No reproducibility analysis; No comparison with reference model/radiologists; No machine learning training; No available code
Malinauskaite et al., 2020 [68]	MRI (T1)	38 pts from 1 center (14 LPSs)	–	SVM after PCA	AUC = 0.926, outperformed the 3 radiologists (AUC = 0.685 −0.805)	–	Retrospective; Single center; Small dataset; Inclusion of myxoid liposarcoma and dedifferentiated liposarcoma; No independent test set; No MRI harmonization; No available code
Leporq et al., 2020 [69]	MRI (FS CE-T1)	81 pts from 1 center (40 ALTs)	–	Linear SVM on reproducible relevant 35 RFs	AUC = 0.96	–	Retrospective; Single center; Small dataset; No independent test set; No MRI harmonization; No IBSI-compliant software; No comparison with reference model/radiologists; No available code
Yang et al., 2022 [29]	CT and MRI (T1, T2)	89 pts from 1 center (38 ALTs)	38 pts from another center (20 ALTs)	deep radiomics model using pretrained CNN (ResNet50) on T1 and T2	AUC = 0.995, outperformed clinical model using LDH and patients' age (AUC = 0.652) and handcrafted radiomics models (AUC = 0.895 −0.929 depending on MR sequences)	AUC = 0.950, outperformed clinical model using LDH and patients' age (AUC = 0.504), and handcrafted radiomics model (AUC = 0.531 −0.586 depending on MR sequences)	Retrospective; No MRI harmonization; No comparison with radiologists; No available code
Fradet et al., 2022 [30]	MRI (FS CE-T1)	85 pts from 1 center (45 ALTs)	60 pts from the same center (32 ALTs)	XGBoost on handcrafted RFs batch-corrected with ComBAT	AUC = 0.99, outperformed model based on pre-trained ResNet50 deep RFs (AUC = 0.80) and non-batch corrected handcrafted radiomics model (AUC = 0.83)	AUC = 0.80, outperformed model based on pre-trained ResNet50 deep RFs (AUC = 0.64) and non-batch corrected handcrafted radiomics model (AUC = 0.70)	Retrospective; Single center; No comparison with radiologists; No available code

(*continued on next page*)

Table 3 (*Continued*)

Author [ref. #]	Imaging modality	No. of patients in training cohort	No. of patient in test cohort	Best model	Performances in training cohort	Performances in validation cohort	Main limitations
Cay et al., 2022 [70]	MRI (T1)	65 pts from 1 center (20 ALTs)	–	SVM trained on reproducible RFs	AUC = 0.987	–	Retrospective; Single center; Small dataset; No independent test set; No comparison with reference model/ radiologists; No available code[§]
Tang et al., 2022 [34]	MRI (T1, FS T2)	97 pts from 1 center (25 ALTs)	25 pts from the same center (7 ALTs)	Random forests trained on selected RFs (using ANOVA and LASSO) from T1 and FS T2	AUC = 0.983, significantly outperformed radiologists (AUC = 0.815–0.884, depending on the 3 radiologists), but not significantly	AUC = 0.968, outperformed radiologists (AUC = 0.889–0.929, depending on the 3 radiologists), but not significantly	Retrospective; Single center; No correction for imbalanced dataset; No IBSI-compliant software; No reproducibility analysis; No available code
Sudjai et al., 2023 [71]	MRI (T1)	70% of the 68 pts from 1 center [§] (with a total of 30 ALTs)	70% of the 68 pts from the same center [§]	LASSO logistic regression on reproducible RFs and tumor-to-bone distance	–	MSK radiologists showed higher diagnostic performances compared to the best model (AUC = 0.91 - 0.94, versus AUC = 0.88).	Retrospective; Single center; Small dataset; No correction for imbalanced dataset; No available code
Foreman et al., 2023 [32]	MRI (T1, T2, FS CE T1)	257 pts from 1 center (65 ALTs)	50 pts from another center (20 ALTs)	LASSO logistic regression on reproducible RFs from all MRI sequences and after PCA and SMOTE	AUC = 0.88	AUC = 0.88, outperformed residents (accuracy = 76% vs. 60–70%) but not senior radiologist (accuracy = 90%)	Retrospective
Gitto et al., 2023 [33]	MRI (T1, T2)	114 pts from 2 centers (50 ALTs)	36 pts from one anther center (12 ALTs)	Random forests model on 8 RFs	AUC = 0.73, accuracy = 67%	Accuracy = 53%, not significantly better than the radiological analysis (accuracy = 64%).	Retrospective; No MRI harmonization; No available code

ALT indicates atypical lipomatous tumor; AUC indicates area under the ROC curve; ANOVA indicates analysis of variance; CE indicates contrast-enhanced; CNN indicates convolutional neural network; FS indicates fat-suppressed; IBSI indicates imaging biomarker standardization initiative, LASSO indicates least absolute shrinkage and selection operator; LDH indicates lactate dehydrogenase, No. indicates number; PCA indicates principal component analysis indicates pts indicates patients; RF indicates radiomics feature; SMOTE indicates synthetic minority oversampling technique; SVM indicates support vector machine.

[§] : Data from the abstract because of non available article despite request to the authors.

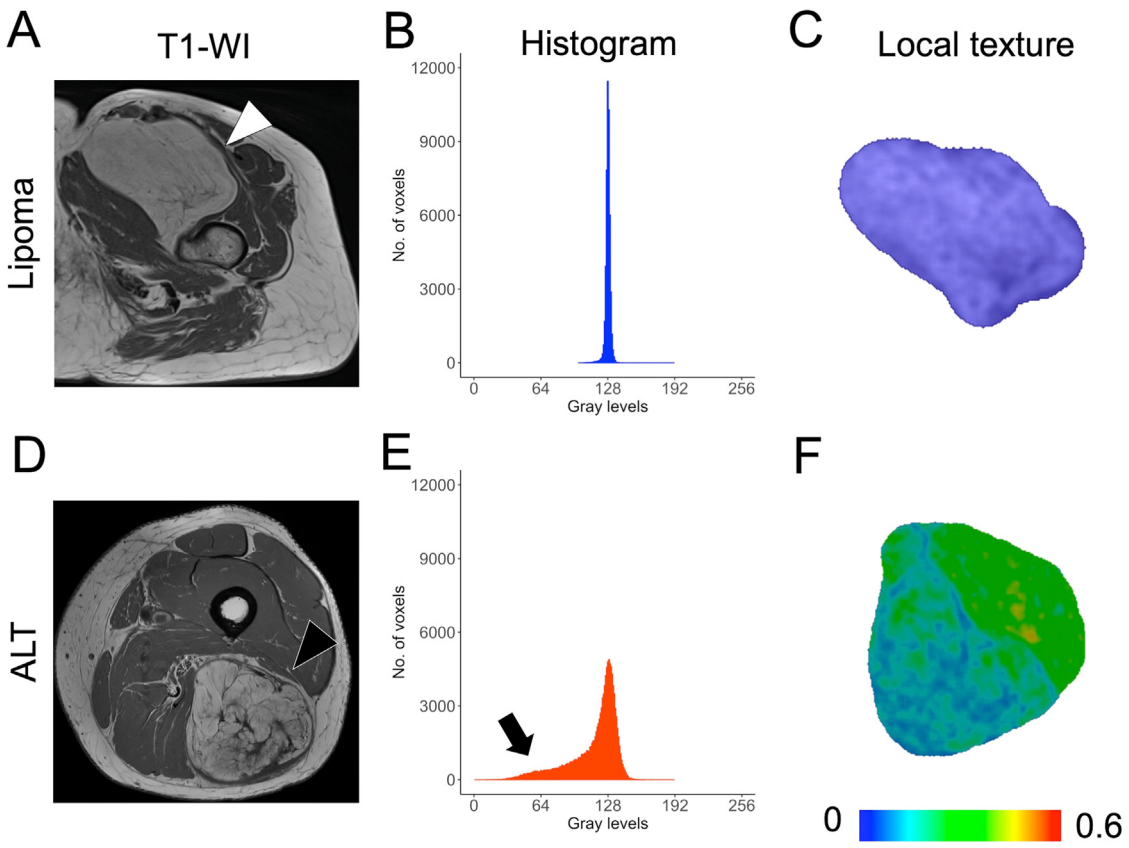

Fig. 3. Differentiation between lipoma and atypical lipomatous (ALT, or well-differentiated liposarcoma) tumor with radiomics. (A, B, C) 73-year-old woman with a 15-cm long deep soft tissue tumor of the left thigh following the iliopsoas muscle. A, on T1-weighted image in the axial plane, the tumor shows a homogeneous fatty signal (white arrowhead) . (B) The histogram of the signal intensities (SIs) on T1-weighted image shows a single peak and no tail. (C) The local texture map for gray level co-occurrence matrix (GLCM) homogeneity (calculated using a 5 × 5 kernel) confirms homogeneous texture. Pathological analysis with MDM2 fluorescence in situ hybridization revealed a lipoma. (D, E, F) 69-year-old woman with a 16-cm long deep soft tissue tumor of the posterior compartment of the left thigh. D, On T1-weighted image in the axial plane, the tumor harbors a main adipocytic signal but several septa of various thicknesses (blackarrowhead). (E) Histogram of SIs on T1-weighted image in the axial plane revealed a skewed distribution with a left tail indicating a large range of lower SIs (*i.e.*, non adipocytic, arrow). (F) The local texture map for GLCM homogeneity confirmed a heterogeneous lesion. Pathological analysis with MDM2 fluorescence in situ hybridization confirmed an ALT with MDM2 amplification.

The same limitations apply to these studies, namely: retrospective design, no data or code sharing, no systematic comparisons to state-of-the-art radiological analysis and grading, and no systematic validation on an independent validation cohort.

In addition to histologic grade, other authors have trained radiomics models to predict Ki-67 index although the interest of Ki-67 has not been proven for STS, contrary to other cancers such as neuroendocrine tumors [40]. Furthermore, radiomics patterns may be associated with the immune landscape of undifferentiated pleomorphic sarcomas (UPS) the most frequent and one of the most aggressive histotype of STS [41]. After developing an unsupervised and explainable classification of 41 UPS based on transcriptomics data secondarily explained with immunohistochemistry, differential gene expression and pathway analyses, immune-high and immune-low subgroups were identified. In parallel, an unsupervised classification of STS based on reproducible texture RFs from CE-T1-WI was developed. The authors found a significant association between radiomics classification and immune classification (P = 0.005), which could pave the way for potential radiomics biomarkers of the sensitivity to immune checkpoint inhibitor in STS.

Lastly, the evolution patterns of STS, as quantified via a delta-radiomics features (ΔRFs) has been correlated with gene-expression profiles in a retrospective single-center cohort of 63 patients [42]. Since STS patients often undergo several MRIs during the diagnostic interval because of their rarity and to the difficulty to reach a correct diagnosis, researchers have studied the 'natural' change in the radiophenotypes of STS during two pre-treatment consecutive MRIs (Fig. 4). They calculated the numeric variation between the RFs from these MRI and developed a robust unsupervised classification of STS depending on their ΔRFs, which provided. Secondly, they explained this classification through the assessment of associations with radiologic semantic features, differential gene expression, oncogenetic pathway analyses and survival analyses. Overall, the authors identified three ΔRFs groups (named A, B and C), including one group (B) that displayed strong increases in intra-tumoral heterogeneity, necrotic signal, peritumoral enhancement, edema and infiltrative margins (all those features being known to correlate with worse outcome). This same group B was characterized by a decrease in apoptosis, an increase in cell proliferation and a decrease in immune response (566 and 1466 differentially-expressed genes in the entire groups and in the subgroup of UPS, respectively). Although limited in size, this study is the first to report direct and explainable relationships between radiomics and transcriptomics data in STS.

5. Predicting response to neoadjuvant treatments

An increasing number of patients with locally-advanced STS are treated with neoadjuvant treatments, including NACT and/or NART because of increasing evidence that they facilitate surgery, increase the rate of R0 surgery, and decrease the risk of metastatic and local relapses [43]. The last ESMO guidelines recommend considering these options in patients with high-risk grade II or III STS, (*i.e.*, after risk assessment

Table 4
Main radiomics studies regarding the identification of high-grade soft tissue sarcomas.

Author [ref.#]	Imaging modality	No. of patients in training cohort	No. of patient in test cohort	Best model	Performances in training cohort	Performances in validation cohort	Main limitations
Corino et al., 2018 [37]	MRI (ADC)	19 pts from 1 center (14 with grade III STS)	–	Model using k-nearest neighbor on 3 RFs from each feature family	AUC = 0.87	–	Retrospective; Single center; Small dataset; No independent test set; No resampling scheme; No IBSI-compliant software; No reproducibility analysis; No comparison with reference model/radiologists; No available code
Peeken et al., 2019 [55]	MRI (FS T2 and CE-T1)	122 pts from 1 center (83 with grade II or III STS)	103 pts from another center (74 with grade II or III STS)	Model using LASSO-penalized logistic regression on fat suppressed T2; OS prognostic model using nomogram based on the T2-based radiomics score for grade and AJCC staging.	For grade prediction: AUC = 0.77. For OS prediction: C-index = 0.76; outperforms clinical models	For grade prediction: AUC = 0.78. For OS prediction: C-index = 0.74; outperforms clinical models	Retrospective; No correction for imbalanced dataset; Grade possibly assessed on biopsy at risk of sampling bias; No comparison with reference model/radiologists; No available code
Zhang et al., 2019 [72]	MRI (FS T2)	35 pts from 1 center (26 with grade II or III STS)	–	Model using SVM on 5 RFs selected with LASSO	AUC = 0.92	–	Retrospective; Single center; Small dataset; No independent test set; No MRI harmonization; No correction for imbalanced dataset; No IBSI-compliant software; No reproducibility analysis; No comparison with reference model/radiologists; No available code
Yan et al., 2021 [73]	MRI (T1, FS T2)	109 pts from 1 center (50 grade III STS)	71 pts from another center (37 grade III STS)	Radiomics score (using logisitic regression on RFs selected with LASSO from T1 and fat suppressed T2); Nomogram including radiomics score, margin definition and AJCC staging	AUC = 0.85 for the radiomics score and 0.92 for the nomogram (outperformed the clinical model with AUC = 0.79);	AUC = 0.83 for the radiomics score and 0.88 for the nomogram (clinical model with AUC = 0.83); C-index for PFS of the radiomics nomogram = 0.58 versus 0.53 for AJCC staging	Retrospective; No resampling scheme; No comparison with radiologists; No available code
Navarro et al., 2021 [38]	MRI (FS T2 and CE-T1)	148 pts from 1 center (96 grade II and III STS)	158 pts from another center (132 grade II and III STS)	Deep learning model using DenseNet161 architecture on FS T2	–	AUC = 0.76; ouperfotmed a model based on clinical features + volume (AUC = 0.57)	Retrospective; No correction for imbalanced dataset; No IBSI-compliant software; Grade assessed on biopsy at risk of underestimation; Deep RFs assessed on single 2D slice at risk of sampling bias; No reproducibility analysis; No comparison with radiologists
Yang et al., 2022 [39]	MRI (T1, FS T2)	540 pts from 1 center (309 with grade II or III STS) splitted into training and testing sets but effectives are not detailed	540 pts from 1 center (309 with grade II or III STS) splitted into training and testing sets but effectives are not detailed	Nomogram including (1) deep RFs extracted from multiple CNN, (2) hand-crafted RFs and (3) size and location, and mined with support vector machines (with radial kernel)	AUC = 0.87; outperformed clinical model (AUC = 0.57) and hand-crafted radiomics models (AUC = 0.85, on T1-based RFs); correlated with overall survival	AUC = 0.85; outperformed clinical model (AUC = 0.52) and hand-crafted radiomics models (AUC = 0.83, on T1-based RFs); correlated with overall survival	Retrospective;; No resampling scheme; No correction for imbalanced dataset; Unclear management of 3D tumor volume in deep learning analysis; Unclear depiction of training and validation cohorts; No comparison with radiologists; No available code

AJCC indicates American Joint Committee on Cancer; AUC indicates area under the ROC curve; CE indicates contrast-enhanced; CNN indicates convolutional neural network; FS indicates fat-suppressed; IBSI indicates imaging biomarker standardization initiative; LASSO indicates least absolute shrinkage and selection operator; No. indicates number; OS indicates overall survival; PCA indicates principal component analysis; pts indicates patients; RF indicates radiomics feature; SMOTE indicates synthetic minority oversampling technique; STS indicates soft tissue sarcoma; SVM indicates support vector machine.

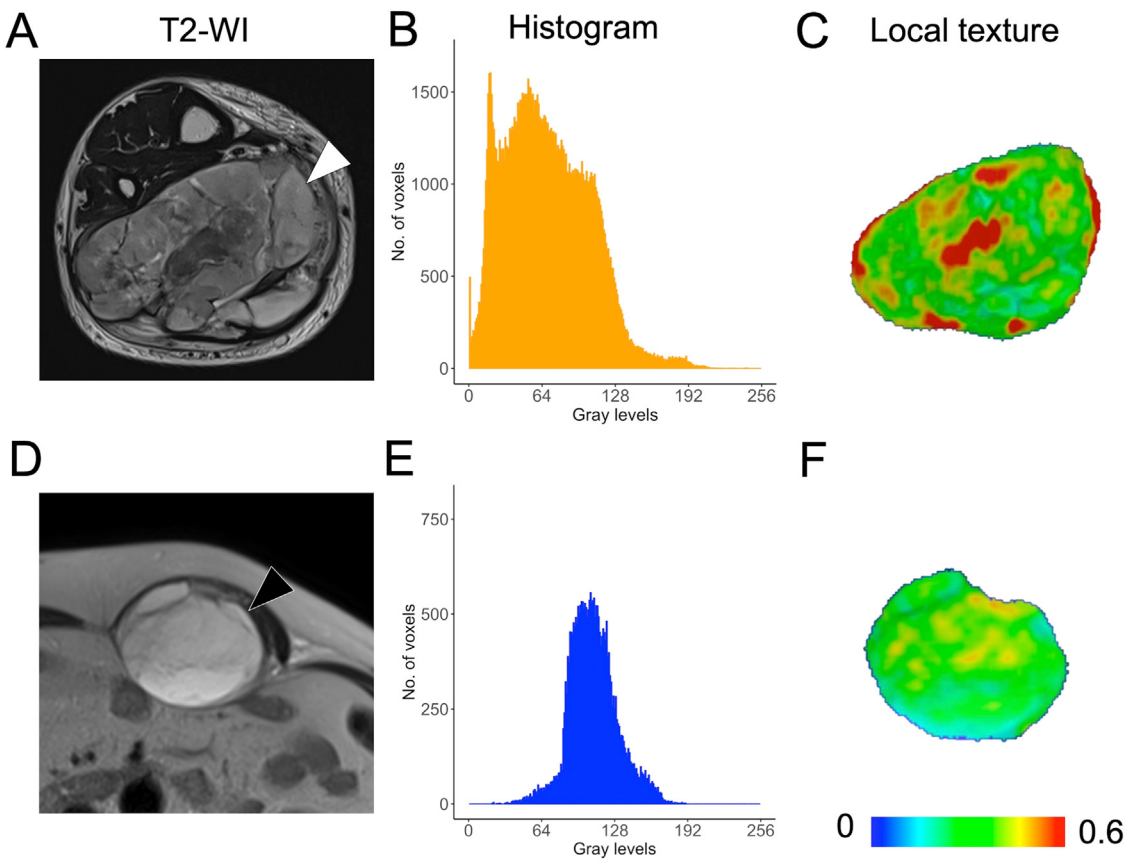

Fig. 4. Identification of high-grade soft-tissue sarcoma and lower survival with radiomics. (A, B, C) 52-year-old man with a locally-advanced 17-cm long deep soft tissue tumor of the posterior compartment of the right calf showing marked heterogeneity on T2-weighted image) (white arrowhead). (B) Histogram of the signal intensities on T2-weighted image shows a wide asymmetric distribution with multiple peaks. (C) The local texture map for gray level co-occurrence matrix (GLCM) homogeneity (calculated using a 5 × 5 kernel) confirms a heterogeneous tumor. Pathological analysis confirmed a grade III (high) undifferentiated pleomorphic sarcoma. The patient had a metastatic relapse 4 months after the end of treatments and died of his disease 15 months later. (D, E, F) 54-year-old woman with a 9.5-cm long deep soft-tissue tumor of the left abdominal wall. D On T2- weighted image the tumor displays a rather homogeneous SIs except for thin septa (black arrowhead). (E) The histogram of SIs shows an almost normal distribution. (F) The local texture map for GLCM homogeneity shows a homogeneous texture. Pathological analysis revealed a grade II (intermediate) undifferentiated pleomorphic and fusiform sarcoma. The patient is still alive 11 years later with no relapse.

according to the SARCULATOR nomogram, for instance), which relies on grade, histologic type, tumor size and patients' age [8,9], but, unfortunately, not on imaging-based characteristics. The response evaluation criteria in solid tumor (RECIST) v1.1 are the reference for the evaluation of tumor response in clinical trials and routine practice, although they are inherently limited in the neoadjuvant setting to a simple relative variation in the longest diameter [44]. Such evaluation cannot capture the early architectural changes due to the entanglement of fibrotic, necrotic and immune processes undergoing at the cellular level, before dimensional reduction, whereas RFs and more particularly ΔRFs have this potential (Fig. 5) [45].

Table 5 shows the six main studies on this topic, with a total of 355 included patients. A main issue is the lack of a consensual definition for the histologic response in STS, with various cut-offs of stainable tumor cells on post-NACT/NART surgical specimens (5%, 10% or 50% depending on studies) – although a recent study suggests a 5% threshold should be applied [46].

All but one found encouraging results, with AUC = 0.80–0.95 in the training cohort. Three studies investigated standard NACT [45,47,48], one NART+NACT [49], one NART alone [50], and one NART + tyrosine kinase inhibitor [51]. Indeed, Fields et al. considered their results as negative with an AUC = 0.45 without any reduction of the high dimensionality of their dataset comprising 1708 RFs and ΔRFs for 44 patients [48]. Yet, when selecting features with $P \leq 0.01$, the AUC of their ADABOOST model increased to 0.82, which remains to be confirmed using cross-validation in their unique cohort or on an independent test set. In fact, only two studies confirmed their results in independent test set and found lower performances suggesting models' overfitting (AUC = 0.63–0.75) [45,49].

Half of those studies compared their findings with those of RECIST v1.1. or American Joint Committee on Cancer staging and systematically found superior performances, except for in one independent test set (similar AUC). In addition to common limitations in radiomics studies, the lack of correction for highly imbalanced datasets must be emphasized. Good histologic response is uncommon (< 20% of all patients), which requires methods to up-sample the minority class (herein, good responders), such as synthetic minority oversampling technique used by Peeken et al. [49,53].

6. Predicting survivals

Lastly, predicting patients' survivals from baseline RFs thanks to survival machine-learning models, or at a given time point thanks to classification models, has been the aim of 14 studies, all retrospective, in 1484 patients. Although debated, the measure of performances in thesurvival model is generally the Harrell concordance index (C-index), which ranges from 0 (worst predictive model) to 1 (perfect model) with 0.5 indicating a non-informative model. The main studies are summarized in Table 6. They mostly involved conventional MRI, although two of them were based on CT-scan and three for

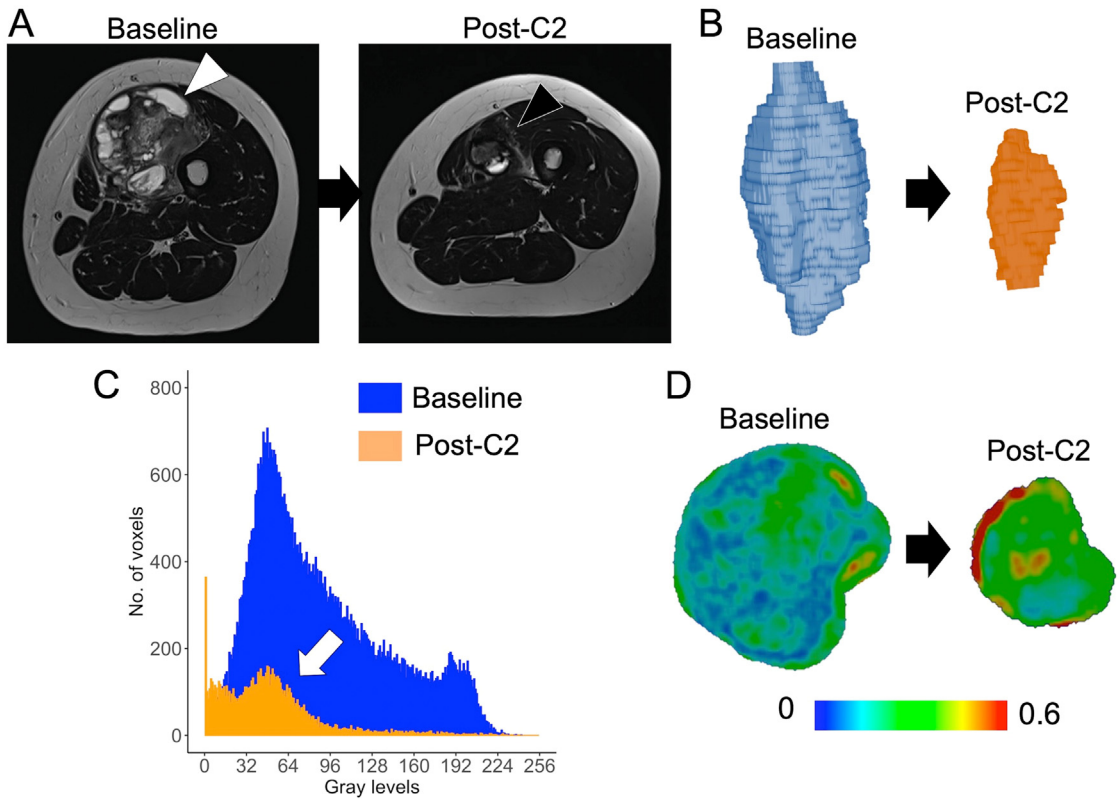

Fig. 5. Identification of good responder to neoadjuvant anthracyclines-based chemotherapy (NACT) with radiomics. Example of a 74-year-old woman with a deep-seated, high grade undifferentiated pleomorphic sarcoma of the thigh. (A) On axial T2-weighted images), the tumor (arrowhead) demonstrates decreases of its longest diameter and signal intensities (SIs) suggesting occurrence of fibrosis after two cycles of NACT (Post-C2). (B) Its volume and shape complexity also decreased. (C) The distribution of SIs fro T2-WI demonstrates a flattening and decay of the histogram towards the left, (i.e., lower Sis; arrow). (D) The local texture map for gray level co-occurrence matrix homogeneity (built with a 5 × 5 kernel) shows a change in the tumor gray level rearrangement. Pathological analysis revealed a grade II (intermediate) undifferentiated pleomorphic and fusiform sarcoma. The pathological analysis of the surgical specimen after six cycles of NACT revealed a good histologic response (< 5% residual tumor cells). The patient is still alive 3.5 years later with no relapse.

them were based on the Cancer Imaging Archive dataset, which includes baseline PET/CT and MRI data of 51 patients. Six of them used an external validation, which systematically validated their results [39,53–57]. Overall, C-indices in the training sets ranged between 0.66 and 0.98 for OS, 0.71 and 0.94 for MFS. In the external validation sets, they were between 0.45 and 0.84 for OS, and between 0.68 and 0.73 for MFS. When comparisons were performed against radiological models, histologic grading and clinical data alone, the radiomics models were systematically more efficient. One study investigated deep radiomics features from ResNet34 to predict recurrence free survival, which contributed to the best model when combined with handcrafted RFs and clinical-radiological features (C-index = 0.87 in training cohort and 0.77 in validation cohort) [56]. However, it must be emphasized that those models were never compared against the nomogram of reference for predicting patients' OS and MFS and stratifying treatments in the last ESMO guidelines, namely the SARCULATOR nomogram [9].

7. Perspectives

Several improvements are expected regarding the use of artificial intelligence to better leverage imaging data of STS patients. First, as manual segmentation is a major bottleneck for the clinical use of radiomics models, automated segmentation tools for CT and MRI relying on CNN such as 3D-U-NET are needed. So far, the deep radiomics models only re-exploited manual segmentations initially performed for handcrafted radiomics. It has been successfully applied to segment retroperitoneal sarcoma and STS on CT, and lipomatous STT on MRI [58–60].

Second, once published, radiomics models are never re-employed on new prospective data. The reasons are the lack of user-friendly application for clinical radiologist and the lack of open-access code to replicate those models in external centers. Moreover, prospective radiomics trials, with clinical decisions depending on the predictions made by radiomics should be designed in order to investigate the real clinical added value of radiomics models. Such trials must rely on accurate models built from retrospective analyses, but those analyses are always biased by treatment strategies stratified on conventional, mainly histologic grade, prognostic factors. Independent and open-access well-annotated datasets would be helpful to establish an objective assessment of the performances of radiomics models for the public, which is an aim of CHAIMELEON [61].

Third, there is a need to better explain the results of radiomics approaches at other scales, by investigating, for instance: (*i*), the relationships between usual radiological features and significant radiomics features or radiomics groups, such as RFs quantitative maps to spatially interpret radiomic models [62] and (*ii*), the relationships with gene-expression signature (such as the Complexity Index in SARComa [CINSARC] signature) [63], gene-expression profiles, oncogenetic pathways and markers of the tumor micro-environment [64]. This would increase the confidence that researchers can provide to such empirical approaches as radiomics (i.e., not driven by hypothesis but by data), and reduce the fear of unexplainable 'black box' algorithms.

Table 5
Main radiomics studies regarding the prediction of response to neoadjuvant treatments in patients with soft-tissue sarcoma.

Author [ref. #]	Question(s)	Imaging modality	No. Of patients in training cohort	No. Of patient in test cohort	Best model	Performances in training cohort	Performances in validation cohort	Main limitations
Crombé et al., 2019 [45]	Prediction of histologic response (<10% viable cells on surgical specimen) following NACT in high grade STS using ΔRFs.	MRI (T2) at baseline and after 2 out of 6 cycles of NACT	50 pts from 1 center (13 good responders)	15 pts from same center (3 good responders)	Random forests algorithm on optimized combinations of ΔRFs and semantics radiologic features	AUC = 0.86, accuracy = 88.1%, higher than RECIST v1.1 (AUC = 0.66, accuracy = 76%)	AUC = 0.63, accuracy = 74.6%, no better than RECIST v1.1 (AUC = 0.72, accuracy = 73.3%)	Retrospective; Single center; Small dataset; No MRI harmonization; No correction for imbalanced dataset; No IBSI-compliant software; No reproducibility analysis; No available code
Crombé et al., 2019 [47]	Prediction of histologic response (<10% viable cells on surgical specimen) following NACT in high grade STS using radiomics from DCE-MRI. Influence of temporal parameters of DCE-MRI sequence on response prediction	MRI (DCE-MRI) at baseline	25 pts from 1 center (5 good responders), prospective cohort.	–	Stepwise logistic regression on pre-treatment RFs from Ktrans and AUC from DCE-MRI sequence lasting 5 min at a temporal resolution of 6 s	AUC = 0.90	–	Single center; Small dataset; No independent test set; No resampling scheme; No correction for imbalanced dataset; No IBSI-compliant software; No reproducibility analysis; No comparison with reference model/radiologists; No available code
Gao et al., 2020 [50]	Prediction of histologic response (<50% viable cells on surgical specimen) using RFs (at baseline, after 3rd fraction and after NART) and ΔRFs.	MRI (ADC)	30 pts from 1 center (unclear no. of good responders)	–	Model using SVM and radiomics and delta-radiomics assessed at the 3 time points	AUC = 0.91, accuracy = 92%	–	Retrospective; Single center; Small dataset; No independent test set; No MRI harmonization; No correction for imbalanced dataset; No available code
Peeken et al., 2021 [49]	Prediction of histologic response (<5% viable cells on surgical specimen) using RFs (before and after NART) and ΔRFs.	MRI (fat suppressed T2, CE-T1)	102 pts from 1 center (11 good responders)	59 pts from another center (5 good responders)	Random forests algorithm on combination of ΔRFs from all sequences, using SMOTE for imbalanced dataset	AUC = 0.80 (higher than RECIST v1.1, AJCC, pre and post-treatment RFs)	AUC = 0.75 (higher than RECIST v1.1, AJCC, pre and post-treatment RFs)	Retrospective
Fields et al., 2023 [48]	Prediction of response to NACT based on ΔRFs	MRI at baseline and after two cycles of NACT	44 pts from 1 center (23 good responders)	–	Adaboost on pre-filtered ΔRFs with $P<0.01$ at univariable analysis	AUC = 0.45 (without pre-filtering) to 0.82 (after pre-filtering ΔRFs with $P \leq 0.01$)	–	Retrospective; Single center; No data harmonization; No reproducibility analysis; No independent test set; No clear definition of response; No detail about MRI sequence on which the radiomics pipeline was conducted; No comparison with other models or reference for response evaluation
Miao et al., 2023 [51]	Prediction of response to TKI + NART based on ΔRFs ± pre-NART RFs ± post-NART RFs	MRI (fat suppressed T2, fat suppressed CE-T1, ADC)	30 pts from 1 center (5 good responders)	–	Only one tested alogorithm: stepwise logistic regression. Best model relying on ΔRFs + pre-NART RFs + post-NART RFs	AUC = 0.95, higher than pre-treatment AJCC (AUC = 0.52) and RECIST v1.1 (AUC = 0.52)	–	Single center; No data harmonization; No independent test set; No resampling method; No correction for highly imbalanced dataset.

AJCC indicates American joint committee on cancer; ADC indicates apparent difusion coefficient; AUC indicates area under the ROC curve; CE indicates contrast-enhanced; ΔRFs indicates delta radiomics features; IBSI indicates imaging biomarker standardization initiative; LASSO indicates least absolute shrinkage and selection operator; NART indicates neoadjuvant radiotherapy; NACT indicates neoadjuvant chemotherapy; pts indicates patients; RECIST indicates response evaluation criteria in solid tumor; RF indicates radiomics features; SMOTE indicates synthetic minority oversampling technique [52]; STS indicates soft-tissue sarcoma.

Table 6
Main radiomics studies regarding the prediction of survival of patients with soft-tissue sarcoma.

Author [ref. #]	Question(s)	Imaging modality	No. of patients in training cohort	No. of patient in test cohort	Best model	Performances in training cohort	Performances in validation cohort	Main limitations
Vallières et al., 2015[§] [11]	Prediction of lung metastastic relapse in STS pts. Methods to optimize fusion of PET and MR imaging. Influence of processing on predictions.	Fusion of PET-CT and MRI (T1, FS T2)	51 pts from the TCIA dataset	–	Logistic regression on 4 optimized texture features.	AUC = 0.98	–	Retrospective; Small dataset; No independent test set; No IBSI-compliant software; No reproducibility analysis; No comparison with reference model/ radiologists
Peeken et al.,2019 [69]	Prediction of LFS, MFS and OS in STS pts treated with NART	CT (with and without injection)	83 pts from one center	87 pts from a 2nd center and 42 pts from a 3rd center	Cox regression tested only, on top 10 RFs, after feature selection based on robustness, no correlation, andunivariable tests.	C-index = 0.72 for OS, C-index = 0.64 for MFS, and C-index = 0.56 for LFS.	C-index = 0.73 and 0.59 for OS, C-index = 0.68 & 0.73 for MFS, and C-index = 0.77 & 0.15 for LFS.	Retrospective; No available code; Bias due to the inclusion of CE and non—CE CT
Crombé et al., 2020 [74]	Prediction of metastatic relapse at 2 years in pts treated with NACT; influence of signal intensity harmonization methods on prediction.	MRI (T2)	50 pts from one center (21 metastatic relapses at 2 years)	20 patients from same center (8 metastatic relapses at 2 years)	Elasticnet logistic regression only tested, with signal intensity harmonization based on histogram matching with average histogram of the population	AUC = 0.71	AUC = 0.77	Retrospective; Single center; Small dataset; No IBSI-compliant software; No reproducibility analysis; No available code
Crombé et al., 2020 [54]	Prediction of MFS in myxoid/ round cells liposarcomas	MRI (T2)	35 pts from 1 center	–	LASSO Cox regression only tested on prefiltered RFs, in order to provide a radiomics score combined with radiological features	C-index = 0.94	–	Retrospective; Single center; Small dataset; No independent test set; No IBSI-compliant software; No reproducibility analysis; No available code
Crombé et al., 2020 [75]	Prediction of MFS in STS pts treated with NACT. Development of methods to quantify the intra-tumoral heterogeneity in neoangiogenesis using DCE-MRI.	MRI (T2, DCE-MRI)	50 pts from 1 center	–	LASSO cox regression only tested, based on combinationof radiological features and RFs from T2 and raw phases of DCE-MRI	C-index = 0.84**;** Better performance with radiomics directly extracted from raw DCE-MRI data than from parametric maps.	–	Retrospective; Single center; Small dataset; No independent test set; No available code
Yang et al., 2021 [76]	Prediction of OS using radiomics after curative treatment.	CT-scan	247 pts from 1 center	106 pts from same center	Random survival forests on pre-selected RFs, and age, lymph node and histologic grade	C-index = 0.78 - 0.86	C-index = 0.45 - 0.60	Retrospective; Single center; No resampling scheme; No MRI harmonization; No IBSI-compliant software; No available code
Peeken et al., 2021 [55]	Prediction of OS using radiomics. Comparison with conventional radiological analysos.	MRI (T1, FS T2)	108 pts from 1 center	71 pts from another center	Elasticnet regression on combination of robust selected T2-based RFs, AJCC staging and age	C-index = 0.66; outperformed semantic features alone and combined	C-index = 0.73; outperformed semantic features alone and combined	Retrospective; No available code
Chen et al., 2021 [77]	Prognostication of STS treated with NART using radiomics (MFS)	MRI (FS T2)	62 pts from 1 center and TCIA dataset	–	Nomogram built with Cox regression model based on radiomics score (using LASSO-penalized Cox regression), tumor location and size	C-index = 0.74; outperformed clinical staging and radiomics score alone (C-index = 0.66).	–	Retrospective; Small dataset; No independent test set; No available code
Fadli et al., 2022 [78]	Prognostication of STS using ΔRFs clusters assessing natural tumor evolution (LFS, MFS, OS)	MRI (CE-T1)	68 pts from 1 center	–	Unsupervised classification based on logarithmic changes in RFs before treatment beginning, combined with radiologic features	Unsupervised classification based on logarithmic changes was an independent predictor for LFS	–	Retrospective; Single center; Small dataset; No independent test set; No resampling scheme; No available code

(*continued on next page*)

Table 6 (*Continued*)

Author [ref. #]	Question(s)	Imaging modality	No. of patients in training cohort	No. of patient in test cohort	Best model	Performances in training cohort	Performances in validation cohort	Main limitations
						(P = 0.0393), but not for MFS or OS.		
Liu et al., 2022[§§] [56]	Prediction of recurrence free survival. Comparisons/potentations of handcrafted RFs and deep RFs.	MRI (T1, T2, ± CE-T1)	151 pts from 1 center	131 pts from 2 other centers	Multivariable stepwise Cox regression on selected/pre-filtered/robust deep RFs, handcrafted RFs and clinical and radiological features	C-index = 0.872, outperformed models radiomics model without RFs frome CE-T1, clinical-radiological models, FNCLCC & NCI grading, AJCC staging, Ki67, MSKCC and japanese nomograms)	C-index = 0.766, outperformed models radiomics model without RFs frome CE-T1, clinical-radiological models, FNCLCC & NCI grading, AJCC staging, MSKCC and japanese nomograms)	Retrospective; No resampling scheme; Unclear input in DL modeling (one or more selected slice vs. entire volume); No IBSI-compliant software for handcrafted RFs; No available code
Hu et al., 2022 [57]	Prediction of lung metastastic relapse in STS pts.	MRI (CE-T1)	122 pts from 1 center	32 pts from another center	Nomogram based on radiomics score obtained by combining margin status and dichotomized prediction from logistic regression on reproducible selected features (after univariable filtering, and additional LASSO selection)	AUC = 0.918 (training) and 0.864 (internal validation), outperformed margins alone and radiomics score alone	AUC = 0.843	Retrospective; No comparison with reference model/radiologists; No available code

AJCC indicates American joint committee on cancer; AUC indicates area under the ROC curve; c-index indicates Harrell's concordance index; CE indicates contrast-enhanced; ΔRFs indicates delta radiomics features; FNCLCC indicates French federation of cancer centers; FS indicates fat-supprsesed; IBSI indicates imaging biomarker standardization initiative; LASSO indicates least absolute shrinkage and selection operator; LFS indicates local relapse free survival; MFS indicates metastatic relapse free survival; NART indicates neoadjuvant radiotherapy; NACT indicates neoadjuvant chemotherapy; NCI indicates National Cancer Institute; OS indicates overall survival; pts indicates patients; RF indicates radiomics features, TCIA indicates the cancer imaging archive.

[§] : Two other studies also investigated the STS TCIA dataset for the same question (i.e., prediction of lung metastasis occurrence, another methodological studies by Vallières et al. in 2017 [79], and one study by Zhao et al. in 2022, with lower performances [80]).

[§§] : Another study was performed by the same research group on 242 out of the 282 patients from the study by Liang et al. to predict the occurrence of lung metastasis (i.e. classification instead of survival analysis) [81].

8. Conclusion

To conclude, although rare cancers with 3000 to 5000 new patients each year in France [65], the intra- and inter-tumoral heterogeneity of STS (which translates into imaging) has naturally made them good candidates to develop radiomics models. Consequently, research in radiomics involving STS has expanded to every domain requiring diagnostic imaging, namely differentiating between benign and malignant STTs (in general and particularly for homogeneous adipocytic tumors), predicting histologic grades, response to NART and NACT, and patients' survivals. Although strongly encouraging and, in total, gathering hundreds of patients, it must be acknowledged that none of the radiomics models coming from these studies has led to clinically-validated application. Considering the recent formalisation of radiomics, such a statement does not mean that radiomics has no future but the exact opposite. Indeed, radiomics is at a turning point in its development with increasing documentations and initiatives (such as IBSI) on how to achieve trustful model, increasing open-science, increasing prospective multicentric trials, and building large databases to independently validate radiomics models (such as the CHAIMELEON project and the Cancer Imaging Archive). In addition to these methodological advances, the implementation of deep learning to replace time-consuming segmentation tasks and provide more personalized numeric features, and explanatory approaches involving other '-omics' material (especially transcriptomics data) pave the way for a very exciting and challenging future for radiomics in STS patients

Informed consent and patient details

The authors declare that this article does not contain any personal information that could lead to the identification of the patients.

Funding

This work did not receive any grant from funding agencies in the public, commercial, or not-for-profit sectors.

Contribution of authors

All authors attest that they meet the current International Committee of Medical Journal Editors (ICMJE) criteria for Authorship. All coauthors were involved in inception, data collection, preparation, and editing of this manuscript. The final manuscript has been reviewed and approved for submission by all coauthors involved.

Declaration of Interests

The authors declare that they have no known competing financial interests or personal relationships that could have appeared to influence the work reported in this paper.

CRediT authorship contribution statement

Amandine Crombé: Conceptualization, Validation, Investigation, Resources, Visualization, Supervision, Project administration, Writing – review & editing, Writing – original draft. **Paolo Spinnato:** Conceptualization, Validation, Investigation, Resources, Writing – original draft, Visualization, Supervision, Writing – review & editing. **Antoine Italiano:** Validation, Resources, Writing – review & editing. **Hervé J. Brisse:** Validation, Resources, Writing – review & editing. **Antoine Feydy:** Validation, Resources, Writing – review & editing. **David Fadli:** Validation, Investigation, Resources, Writing – review & editing. **Michèle Kind:** Conceptualization, Validation, Investigation, Resources, Supervision, Writing – review & editing.

References

[1] Fletcher CDM, Bridge JA, Hogendoorn PCW, Martens F. WHO classification of tumours of soft tissue and bone. 5th ed. Lyon, France: IARC Press; 2020.
[2] Crombé A, Marcellin P-J, Buy X, Stoeckle E, Brouste V, Italiano A, et al. Soft-tissue sarcomas: assessment of MRI features correlating with histologic grade and patient outcome. Radiology 2019;291:710–21.
[3] Zhao F, Ahlawat S, Farahani SJ, Weber KL, Montgomery EA, Carrino JA, et al. Can MR imaging be used to predict tumor grade in soft-tissue sarcoma? Radiology 2014;272:192–201.
[4] Crombe A, Alberti N, Stoeckle E, Brouste V, Buy X, Coindre JM, et al. Soft tissue masses with myxoid stroma: can conventional magnetic resonance imaging differentiate benign from malignant tumors? Eur J Radiol 2016;85:1875–82.
[5] Yoo HJ, Hong SH, Kang Y, Choi J-Y, Moon KC, Kim H-S, et al. MR imaging of myxofibrosarcoma and undifferentiated sarcoma with emphasis on tail sign; diagnostic and prognostic value. Eur Radiol 2014;24:1749–57.
[6] Nardo L, Abdelhafez YG, Acquafredda F, Schirò S, Wong AL, Sarohia D, et al. Qualitative evaluation of MRI features of lipoma and atypical lipomatous tumor: results from a multicenter study. Skeletal Radiol 2020;49:1005–14.
[7] Gondim Teixeira PA. The role of the radiologist in the management of soft-tissue masses: with great power comes great responsibility. Diagn Interv Imaging 2023;104:205–6.
[8] Gronchi A, Miah AB, Dei Tos AP, Abecassis N, Bajpai J, Bauer S, et al. Soft tissue and visceral sarcomas: ESMO-EURACAN-GENTURIS clinical practice guidelines for diagnosis, treatment and follow-up. Ann Oncol 2021;32:1348–65.
[9] Callegaro D, Miceli R, Bonvalot S, Ferguson P, Strauss DC, Levy A, et al. Development and external validation of two nomograms to predict overall survival and occurrence of distant metastases in adults after surgical resection of localised soft-tissue sarcomas of the extremities: a retrospective analysis. Lancet Oncol 2016;17:671–80.
[10] Gillies RJ, Anderson AR, Gatenby RA, Morse DL. The biology underlying molecular imaging in oncology: from genome to anatome and back again. Clin Radiol 2010;65:517–21.
[11] Vallières M, Freeman CR, Skamene SR, El Naqa I. A radiomics model from joint FDG-PET and MRI texture features for the prediction of lung metastases in soft-tissue sarcomas of the extremities. Phys Med Biol 2015;60:5471–96.
[12] Lambin P, Leijenaar RTH, Deist TM, Peerlings J, de Jong EEC, van Timmeren J, et al. Radiomics: the bridge between medical imaging and personalized medicine. Nat Rev Clin Oncol 2017;14:749–62.
[13] Limkin EJ, Sun R, Dercle L, Zacharaki EI, Robert C, Reuzé S, et al. Promises and challenges for the implementation of computational medical imaging (radiomics) in oncology. Ann Oncol 2017;28:1191–206.
[14] Boeken T, Feydy J, Lecler A, Soyer P, Feydy A, Barat M, et al. Artificial intelligence in diagnostic and interventional radiology: where are we now? Diagn Interv Imaging 2023;104:1–5.
[15] Zwanenburg A, Vallières M, Abdalah MA, Aerts HJWL, Andrearczyk V, Apte A, et al. The image biomarker standardization initiative: standardized quantitative radiomics for high-throughput image-based phenotyping. Radiology 2020;295:328–38.
[16] Vallières M, Zwanenburg A, Badic B, Cheze Le Rest C, Visvikis D, Hatt M. Responsible radiomics research for faster clinical translation. J Nucl Med 2018;59:189–93.
[17] Orlhac F, Frouin F, Nioche C, Ayache N, Buvat I. Validation of a Method to compensate multicenter effects affecting CT radiomics. Radiology 2019;291:53–9.
[18] Crombé A, Fadli D, Italiano A, Saut O, Buy X, Kind M. Systematic review of sarcomas radiomics studies: bridging the gap between concepts and clinical applications? Eur J Radiol 2020;132:109283.
[19] Crombé A, Kind M, Fadli D, Miceli M, Linck PA, Bianchi G, et al. Soft-tissue sarcoma in adults: imaging appearances, pitfalls and diagnostic algorithms. Diagn Interv Imaging 2023;104:207–20.
[20] Lacroix M, Aouad T, Feydy J, Biau D, Larousserie F, Fournier L, et al. Artificial intelligence in musculoskeletal oncology imaging: a critical review of current applications. Diagn Interv Imaging 2023;104:18–23.
[21] Pan SJ, Yang Q. A survey on transfer learning. IEEE Trans Knowl Data Eng 2010;22:1345–59.
[22] Kransdorf MJ, Murphey MD. Imaging of soft-tissue musculoskeletal masses: fundamental concepts. Radiographics 2016;36:1931–48.
[23] Juntu J, Sijbers J, De Backer S, Rajan J, Van Dyck D. Machine learning study of several classifiers trained with texture analysis features to differentiate benign from malignant soft-tissue tumors on T1-weighted MR images. J Magn Reson Imaging 2010;31:680–9.
[24] Fields BKK, Demirjian NL, Hwang DH, Varghese BA, Cen SY, Lei X, et al. Whole-tumor 3D volumetric MRI-based radiomics approach for distinguishing between benign and malignant soft tissue tumors. Eur Radiol 2021;31:8522–35.
[25] Lee SE, Jung JY, Nam Y, Lee SY, Park H, Shin SH, et al. Radiomics of diffusion-weighted MRI compared to conventional measurement of apparent diffusion-coefficient for differentiating between benign and malignant soft tissue tumors. Sci Rep 2021;11:15276.
[26] Yue Z, Wang X, Yu T, Shang S, Liu G, Jing W, et al. Multi-parametric MRI-based radiomics for the diagnosis of malignant soft-tissue tumor. Magn Reson Imaging 2022;91:91–9.
[27] Moulin B, Messiou C, Crombé A, Kind M, Hohenberger P, Rutkowski P, et al. Diagnosis strategy for adipocytic soft-tissue tumors in adults: a consensus from European experts. Eur J Surg Oncol 2022;48:518–25.
[28] Haidey J, Low G, Wilson MP. Radiomics-based approaches outperform visual analysis for differentiating lipoma from atypical lipomatous tumors: a review. Skeletal Radiol 2023;52:1089–100.

[29] Yang Y, Zhou Y, Zhou C, Ma X. Novel computer aided diagnostic models on multi-modality medical images to differentiate well differentiated liposarcomas from lipomas approached by deep learning methods. Orphanet J Rare Dis 2022;17:158.
[30] Fradet G, Ayde R, Bottois H, El Harchaoui M, Khaled W, Drapé JL, et al. Prediction of lipomatous soft tissue malignancy on MRI: comparison between machine learning applied to radiomics and deep learning. Eur Radiol Exp 2022;6:41.
[31] Pressney I, Khoo M, Endozo R, Ganeshan B, O'Donnell P. Pilot study to differentiate lipoma from atypical lipomatous tumour/well-differentiated liposarcoma using MR radiomics-based texture analysis. Skeletal Radiol 2020;49:1719–29.
[32] Foreman SC, Llorián-Salvador O, David DE, Rösner VKN, Rischewski JF, Feuerriegel GC, et al. Development and evaluation of MRI-based radiomic models to differentiate atypical lipomatous tumor from lipoma. Cancers 2023;15:2150.
[33] Gitto S, Interlenghi M, Cuocolo R, Salvatore C, Giannetta V, Badalyan J, et al. MRI radiomics-based machine learning for classification of deep-seated lipoma and atypical lipomatous tumor of the extremities. Radiol Med 2023;128:989–98.
[34] Tang Y, Cui J, Zhu J, Fan G. Differentiation between lipomas and atypical lipomatous tumors of the extremities using radiomics. J Magn Reson Imaging 2022;56:1746–54.
[35] Coindre JM, Terrier P, Bui NB, Bonichon F, Collin F, Le Doussal V, et al. Prognostic factors in adult patients with locally controlled soft tissue sarcoma: a study of 546 patients from the French Federation of Cancer Centers Sarcoma Group. J Clin Oncol 1996;14:869–77.
[36] Trojani M, Contesso G, Coindre JM, Rouesse J, Bui NB, de Mascarel A, et al. Soft-tissue sarcomas of adults: study of pathological prognostic variables and definition of a histopathological grading system. Int J Cancer 1984;33:37–42.
[37] Corino VDA, Montin E, Messina A, Casali PG, Gronchi A, Marchianò A, et al. Radiomic analysis of soft tissues sarcomas can distinguish intermediate from high-grade lesions. J Magn Reson Imaging 2018;47:829–40.
[38] Navarro F, Dapper H, Asadpour R, Knebel C, Spraker MB, Schwarze V, et al. Development and external validation of deep-learning-based tumor grading models in soft-tissue sarcoma using MRI. Cancers 2021;13:2866.
[39] Yang Y, Zhou Y, Zhou C, Zhang X, Ma X. MRI-based computer-aided diagnostic model to predict tumor grading and clinical outcomes in patients with soft tissue sarcoma. J Magn Reson Imaging 2022;56:1733–45.
[40] Yang Y, Zhang L, Wang T, Jiang Z, Li Q, Wu Y, et al. MRI Fat-saturated T2-weighted radiomics model for identifying the Ki-67 index of soft tissue sarcomas. J Magn Reson Imaging 2023;58:534–45.
[41] Toulmonde M, Lucchesi C, Verbeke S, Crombe A, Adam J, Geneste D, et al. High throughput profiling of undifferentiated pleomorphic sarcomas identifies two main subgroups with distinct immune profile, clinical outcome and sensitivity to targeted therapies. EBioMedicine 2020;62:103131.
[42] Crombé A, Bertolo F, Fadli D, Kind M, Le Loarer F, Perret R, et al. Distinct patterns of the natural evolution of soft tissue sarcomas on pre-treatment MRIs captured with delta-radiomics correlate with gene expression profiles. Eur Radiol 2023;33:1205–18.
[43] Italiano A, Stoeckle E. Role of perioperative chemotherapy in soft-tissue sarcomas: it's time to end a never-ending story. Eur J Cancer 2018;97:53–4 1990.
[44] Eisenhauer EA, Therasse P, Bogaerts J, Schwartz LH, Sargent D, Ford R, et al. New response evaluation criteria in solid tumours: revised RECIST guideline (version 1.1). Eur J Cancer 2009;45:228–47.
[45] Crombé A, Périer C, Kind M, De Senneville BD, Le Loarer F, Italiano A, et al. T2-based MRI delta-radiomics improves response prediction in soft-tissue sarcomas treated by neoadjuvant chemotherapy. J Magn Reson Imaging 2019;50:497–510.
[46] Crombé A, Cousin S, Spalato-Ceruso M, Loarer FL, Toulmonde M, Michot A, et al. Implementing a machine learning strategy to predict pathologic response in patients with soft tissue sarcomas treated with neoadjuvant chemotherapy. JCO Clin Cancer Inform 2021;5:958–72.
[47] Crombé A, Saut O, Guigui J, Italiano A, Buy X, Kind M. Influence of temporal parameters of DCE-MRI on the quantification of heterogeneity in tumor vascularization. J Magn Reson Imaging 2019;50:1773–88.
[48] Fields BKK, Demirjian NL, Cen SY, Varghese BA, Hwang DH, Lei X, et al. Predicting soft tissue sarcoma response to neoadjuvant chemotherapy using an MRI-based delta-radiomics approach. Mol Imaging Biol 2023;25:776–87.
[49] Peeken JC, Asadpour R, Specht K, Chen EY, Klymenko O, Akinkuoroye V, et al. MRI-based delta-radiomics predicts pathologic complete response in high-grade soft-tissue sarcoma patients treated with neoadjuvant therapy. Radiother Oncol 2021;164:73–82.
[50] Gao Y, Kalbasi A, Hsu W, Ruan D, Fu J, Shao J, et al. Treatment effect prediction for sarcoma patients treated with preoperative radiotherapy using radiomics features from longitudinal diffusion-weighted MRIs. Phys Med Biol 2020;65:175006.
[51] Miao L, Cao Y, Zuo L, Zhang H, Guo C, Yang Z, et al. Predicting pathological complete response of neoadjuvant radiotherapy and targeted therapy for soft tissue sarcoma by whole-tumor texture analysis of multisequence MRI imaging. Eur Radiol 2023;33:3984–94.
[52] Blagus R, Lusa L. SMOTE for high-dimensional class-imbalanced data. BMC Bioinformatics 2013;14:106.
[53] Peeken JC, Spraker MB, Knebel C, Dapper H, Pfeiffer D, Devecka M, et al. Tumor grading of soft tissue sarcomas using MRI-based radiomics. EBioMedicine 2019;48:332–40.
[54] Crombé A, Le Loarer F, Sitbon M, Italiano A, Stoeckle E, Buy X, et al. Can radiomics improve the prediction of metastatic relapse of myxoid/round cell liposarcomas? Eur Radiol 2020;30:2413–24.
[55] Peeken JC, Neumann J, Asadpour R, Leonhardt Y, Moreira JR, Hippe DS, et al. Prognostic assessment of high-grade soft-tissue sarcoma: comparison between semantic image analysis and radiomics. Cancers 2021;13:1929.
[56] Liu S, Sun W, Yang S, Duan L, Huang C, Xu J, et al. Deep learning radiomic nomogram to predict recurrence in soft tissue sarcoma: a multi-institutional study. Eur Radiol 2022;32:793–805.
[57] Hu Y, Wang H, Yue Z, Wang X, Wang Y, Luo Y, et al. A contrast-enhanced MRI-based nomogram to identify lung metastasis in soft-tissue sarcoma: a multi-centre study. Med Phys 2023;50:2961–70.
[58] Salvaggio G, Cutaia G, Greco A, Pace M, Salvaggio L, Vernuccio F, et al. Deep learning networks for automatic retroperitoneal sarcoma segmentation in computerized tomography. Appl Sci 2022;12:1665.
[59] Marin T, Zhuo Y, Lahoud RM, Tian F, Ma X, Xing F, et al. Deep learning-based GTV contouring modeling inter- and intra-observer variability in sarcomas. Radiother Oncol 2022;167:269–76.
[60] Liu CC, Abdelhafez YG, Yap SP, Acquafredda F, Schirò S, Wong AL, et al. AI-based automated lipomatous tumor segmentation in MR images: ensemble solution to heterogeneous data. J Digit Imaging 2023;36:1049–59.
[61] Bonmatí LM, Miguel A, Suárez A, Aznar M, Beregi JP, Fournier L, et al. CHAIMELEON project: creation of a pan-European repository of health imaging data for the development of AI-powered cancer management tools. Front Oncol 2022;12:742701.
[62] Escobar T, Vauclin S, Orlhac F, Nioche C, Pineau P, Champion L, et al. Voxel-wise supervised analysis of tumors with multimodal engineered features to highlight interpretable biological patterns. Med Phys 2022;49:3816–29.
[63] Chibon F, Lagarde P, Salas S, Pérot G, Brouste V, Tirode F, et al. Validated prediction of clinical outcome in sarcomas and multiple types of cancer on the basis of a gene expression signature related to genome complexity. Nat Med 2010;16:781–7.
[64] Xue C, Zhou Q, Xi H, Zhou J. Radiomics: a review of current applications and possibilities in the assessment of tumor microenvironment. Diagn Interv Imaging 2023;104:113–22.
[65] Honoré C, Méeus P, Stoeckle E, Bonvalot S. Soft tissue sarcoma in France in 2015: epidemiology, classification and organization of clinical care. J Visc Surg 2015;152:223–30.
[66] Thornhill RE, Golfam M, Sheikh A, Cron GO, White EA, Werier J, et al. Differentiation of lipoma from liposarcoma on MRI using texture and shape analysis. Acad Radiol 2014;21:1185–94.
[67] Vos M, Starmans MPA, Timbergen MJM, van der Voort SR, Padmos GA, Kessels W, et al. Radiomics approach to distinguish between well differentiated liposarcomas and lipomas on MRI. Br J Surg 2019;106:1800–9.
[68] Malinauskaite I, Hofmeister J, Burgermeister S, Neroladaki A, Hamard M, Montet X, et al. Radiomics and machine learning differentiate soft-tissue lipoma and liposarcoma better than musculoskeletal radiologists. Sarcoma 2020;2020:7163453.
[69] Leporq B, Bouhamama A, Pilleul F, Lame F, Bihane C, Sdika M, et al. MRI-based radiomics to predict lipomatous soft tissue tumors malignancy: a pilot study. Cancer Imaging 2020;20:78.
[70] Cay N, Mendi BAR, Batur H, Erdogan F. Discrimination of lipoma from atypical lipomatous tumor/well-differentiated liposarcoma using magnetic resonance imaging radiomics combined with machine learning. Jpn J Radiol 2022;40:951–60.
[71] Sudjai N, Siriwanarangsun P, Lektrakul N, Saiviroonporn P, Maungsomboon S, Phimolsarnti R, et al. Tumor-to-bone distance and radiomic features on MRI distinguish intramuscular lipomas from well-differentiated liposarcomas. J Orthop Surg 2023;18:255.
[72] Zhang Y, Zhu Y, Shi X, Tao J, Cui J, Dai Y, et al. Soft tissue sarcomas: preoperative predictive histopathological grading based on radiomics of MRI. Acad Radiol 2019;26:1262–8.
[73] Yan R, Hao D, Li J, Liu J, Hou F, Chen H, et al. MRI-based radiomics nomogram for prediction of the histopathological grade of soft tissue sarcomas: a two-center study. J Magn Reson Imaging 2021;53:1683–96.
[74] Peeken JC, Bernhofer M, Spraker MB, Pfeiffer D, Devecka M, Thamer A, et al. CT-based radiomic features predict tumor grading and have prognostic value in patients with soft tissue sarcomas treated with neoadjuvant radiation therapy. Radiother Oncol 2019;135:187–96.
[75] Crombé A, Fadli D, Buy X, Italiano A, Saut O, Kind M. High-grade soft-tissue sarcomas: can optimizing dynamic contrast-enhanced MRI postprocessing improve prognostic radiomics models? J Magn Reson Imaging 2020;52:282–97.
[76] Yang Y, Ma X, Wang Y, Ding X. Prognosis prediction of extremity and trunk wall soft-tissue sarcomas treated with surgical resection with radiomic analysis based on random survival forest. Updat Surg 2022;4:355–65.
[77] Chen S, Li N, Tang Y, Chen B, Fang H, Qi S, et al. Radiomics analysis of fat-saturated T2-weighted MRI sequences for the prediction of prognosis in soft tissue sarcoma of the extremities and trunk treated with neoadjuvant radiotherapy. Front Oncol 2021;11:710649.
[78] Fadli D, Kind M, Michot A, Le Loarer F, Crombé A. Natural changes in radiological and radiomics features on MRIs of soft-tissue sarcomas naïve of treatment: correlations with histology and patients' outcomes. J Magn Reson Imaging 2022;56:77–96.
[79] Vallières M, Laberge S, Diamant A, El Naqa I. Enhancement of multimodality texture-based prediction models via optimization of PET and MR image acquisition protocols: a proof of concept. Phys Med Biol 2017;62:8536–65.
[80] Zhao W, Huang X, Wang G, Guo J. PET/MR fusion texture analysis for the clinical outcome prediction in soft-tissue sarcoma. Cancer Imaging 2022;22:7.
[81] Liang HY, Yang SF, Zou HM, Hou F, Duan LS, Huang CC, et al. Deep learning radiomics nomogram to predict lung metastasis in soft-tissue sarcoma: a multi-center study. Front Oncol 2022;12:897676.